Journal of Constructional Steel Research 179 (2021) 106576

Contents lists available at ScienceDirect

Journal of Constructional Steel Research

Theoretical evaluation method for the progressive collapse resistance of steel frame buildings

Junjie Wang [a,b], Wei Wang [a,b,*]

[a] State Key Laboratory of Disaster Reduction in Civil Engineering, Tongji University, Shanghai 200092, China
[b] Department of Structural Engineering, Tongji University, Shanghai 200092, China

ARTICLE INFO

Article history:
Received 13 October 2020
Received in revised form 5 February 2021
Accepted 7 February 2021
Available online 17 February 2021

Keywords:
Progressive collapse
Disproportionate collapse
Catenary action
Membrane action
Composite slab

ABSTRACT

Steel-concrete composite slabs are widely adopted in steel frame buildings as the gravity load resisting system. So far, the progressive collapse resistance of this type of structure is mainly evaluated by the experimental or numerical methods, which is complicated, time-consuming and expensive. Hence, in this study, an easy-to-use theoretical method for giving a quick evaluation of the progressive collapse resistance at the design stage is proposed for this type of structure. When the floor system is horizontally constrained at the parallel boundaries, the theoretical model is composed of three stages, i.e., elastic stage, plastic stage, and catenary stage. At the elastic stage and plastic stage, the load is carried by the flexural resistance of the floor system. At the catenary stage, the load is resisted by the catenary action and the tensile membrane action. When the floor system is not constrained at the parallel horizontal boundaries, the theoretical model is only composed of elastic stage and plastic stage. Then, this theoretical model is validated with different experimental and numerical simulation results. Finally, for the multi-story and high-rise buildings, considering the potential instability of columns under the excessively redistributed gravity load, the potentially maximum tributary area of each column under the progressive collapse scenario is presented.

1. Introduction

Steel-concrete composite slabs, attributing to their saving in construction time and excellent durability, are widely used in steel frame buildings as the gravity load resisting system. Besides, when the steel frame buildings subjecting to abnormal loads, the composite floor system is also playing a vital role in progressive collapse prevention, which is supported by the experimental and numerical investigations conducted by Johnson et al. [1], Hadjioannou et al. [2], Fu et al. [3], Zandonini et al. [4], Sadek et al. [5], Alashker et al. [6,7], Li and El-Tawil [8], Jeyarajan and Liew [9]. Compared with the skeleton steel frame (without composite slab), this improvement in progressive collapse prevention is mainly due to the increased flexural resistance from the composite slab, and the composite action between the composite slab and steel beams. The composite action can be inoperative when the composite slab is severely damaged at the large deformation stage. Under this condition, if the floor system is fully constrained at the parallel horizontal boundaries, tensile membrane action can be developed and become a primary source of resistance. For the reinforced concrete slab, the tensile membrane action is provided by the slab reinforcement. For the composite slab, except for the steel reinforcement, the steel deck can also develop tensile membrane force in its longitudinal direction. It is worth noting that the steel deck may contribute more resistance than the steel reinforcement at the large deformation stage [6].

At present, the investigations on progressive collapse resistance of steel frame structures rely mainly on experimental and numerical methods. These two methods are complicated, time-consuming, and expensive, so they cannot quickly evaluate the progressive collapse resistance at the design stage. Hence, an easy-to-use theoretical method is needed to expediently predict the progressive collapse resistance of steel frame structures with composite slab. Up to now, several theoretical models have been proposed by Bailey [10], Alashker et al. [11], Fu et al. [12], Li et al. [13], and Zhang et al. [14]. However, these models require either iterative calculation [11,12], or complex calculation based on stringent assumptions [10,13,14]. Therefore, in this study, a simplified theoretical model is proposed to evaluate the progressive collapse resistance of steel frame structures with composite slab.

2. Theoretical model

As shown in Fig. 1, according to the horizontal boundary conditions, the progressive collapse scenarios subjecting single column loss can be divided into nine types, namely A1, A2, A3, B1, B2, B3, C1, C2, C3. As

* Corresponding author at: State Key Laboratory of Disaster Reduction in Civil Engineering, Tongji University, Shanghai 200092, China.
E-mail address: weiwang@tongji.edu.cn (W. Wang).

https://doi.org/10.1016/j.jcsr.2021.106576
0143-974X/

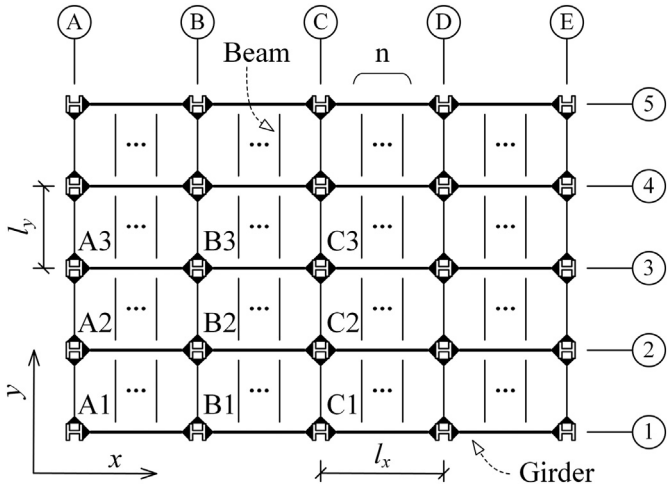

Fig. 1. Column removal scenarios.

the floor system has been horizontally constrained at the parallel boundaries, the A3, B3, C1, C2, and C3 cases can fully develop the catenary action and the tensile membrane action at the large deformation stage. As lacking horizontal constraints, the other four cases (A1, A2, B1, B2) are assumed to only develop the flexural resistance. The derivation of the theoretical model in this section is carried out in accordance with the prototype structure shown in Fig. 1. The girders are arranged in the x direction with a span of l_x, and the beams are arranged in the y direction with a span of l_y. Each girder span has n rows of beams connected to it, and the spacing of the beam is constant. The girder-to-column connection and the beam-to-column connection are rigid connections, and the beam-to-girder connection is a hinged connection.

Fig. 2 (a) is a theoretical model suitable for A1, A2, B1, B2 cases, while Fig. 2 (b) is a theoretical model suitable for A3, B3, C1, C2, C3 cases. ω and δ represent the uniformly distributed load on the floor and the vertical displacement where the column is removed. The load-displacement curve of the theoretical model corresponding to Fig. 2 (b) is divided into three stages: elastic stage, plastic stage, and catenary stage. These three stages are divided by three characteristic displacements, namely δ_y, δ_t and δ_u. δ_y represents the corresponding displacement when the steel beam and composite slab reach the full plastic resistance. According to Eurocode 8 [15], the beam chord rotation angle corresponding to δ_y is 0.013 rad. When the steel beam and composite slab reach the full plastic resistance, the resistance of the entire structure is ω_y. The resistance mechanism gradually changes from the flexural mechanism to the catenary action and the tensile membrane action. When the displacement reaches δ_t, the resultant force of the catenary action and the tensile membrane action exceeds ω_y. After that, the structural load is assumed to be completely carried by the catenary action and tensile membrane action. When the displacement reaches δ_u, the overall structure fails and loses its capacity. For A1, A2, B1, B2 cases, as shown in Fig. 2(a), the load-displacement curve of the theoretical model only includes two stages, namely the elastic stage and the plastic stage.

2.1. Elastic stage

As shown in Fig. 2, before the vertical displacement reaches δ_y, the load-displacement curve of the theoretical model is assumed to be a straight line. In the elastic stage, the structural load is carried by the flexural mechanism of the beam system and the composite slab system. Therefore, ω_y can be calculated by the yield line method. As shown in Fig. 3, the yield line method calculation diagrams corresponding to each column removal cases can be divided into four types: I, II, III, and IV. The solid lines represent the positive yield line, while the dashed lines represent the negative yield line. $\theta_x = \delta/l_x$ and $\theta_y = \delta/l_y$ are the rotation angles of the floor plastic hinge around the y-axis and the x-axis. M_g and M'_g are the full-section plastic flexural capacity of the girder in the positive and negative moment zone. M_b and M'_b are the full-section plastic flexural capacity of the beam in the positive and negative moment zone. m_{sx} and m_{sy} are the full-section plastic flexural capacity of the per unit width composite slab around the y-axis and x-axis in the positive moment zone, while m'_{sx} and m'_{sy} are the full-section plastic flexural capacity of the per unit width composite slabs around the y-axis and x-axis in the negative moment zone.

The internal work $W_{internal}$ corresponding to Type I, Type II, Type III and Type IV is calculated according to Eqs. 1 to 4, respectively.

$$W_{internal} = \left(M'_g + m'_{sx}l_y\right)\theta_x + \left((1+n)M'_b + m'_{sy}l_x\right)\theta_y \tag{1}$$

$$W_{internal} = \left(M'_g + 2m_{sx}l_y + 2m'_{sx}l_y\right)\theta_x + \left(2(1+n)M_b + 2M'_b + 2m_{sy}l_x + 2m'_{sy}l_x\right)\theta_y \tag{2}$$

$$W_{internal} = \left(2M_g + 2M'_g + 2m_{sx}l_y + 2m'_{sx}l_y\right)\theta_x + \left(2nM_b + M'_b + 2m_{sy}l_x + 2m'_{sy}l_x\right)\theta_y \tag{3}$$

$$W_{internal} = \left(2M_g + 2M'_g + 4m_{sx}l_y + 4m'_{sx}l_y\right)\theta_x + \left(2(1+2n)M_b + 2M'_b + 4m_{sy}l_x + 4m'_{sy}l_x\right)\theta_y \tag{4}$$

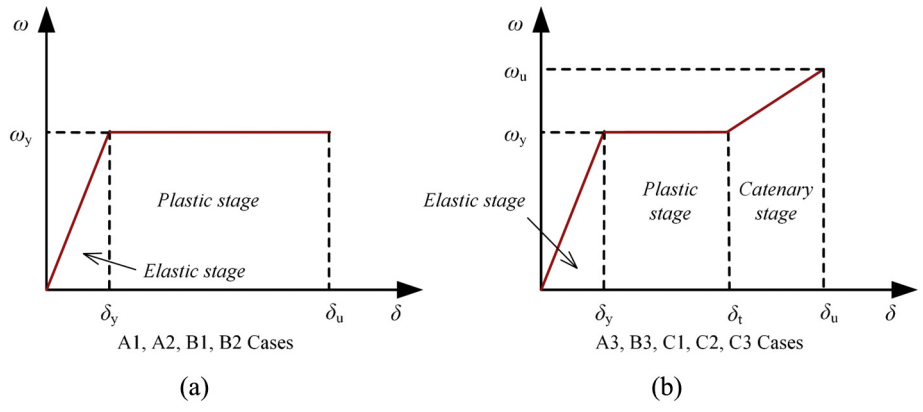

Fig. 2. Theoretical models corresponding to different column removal cases.

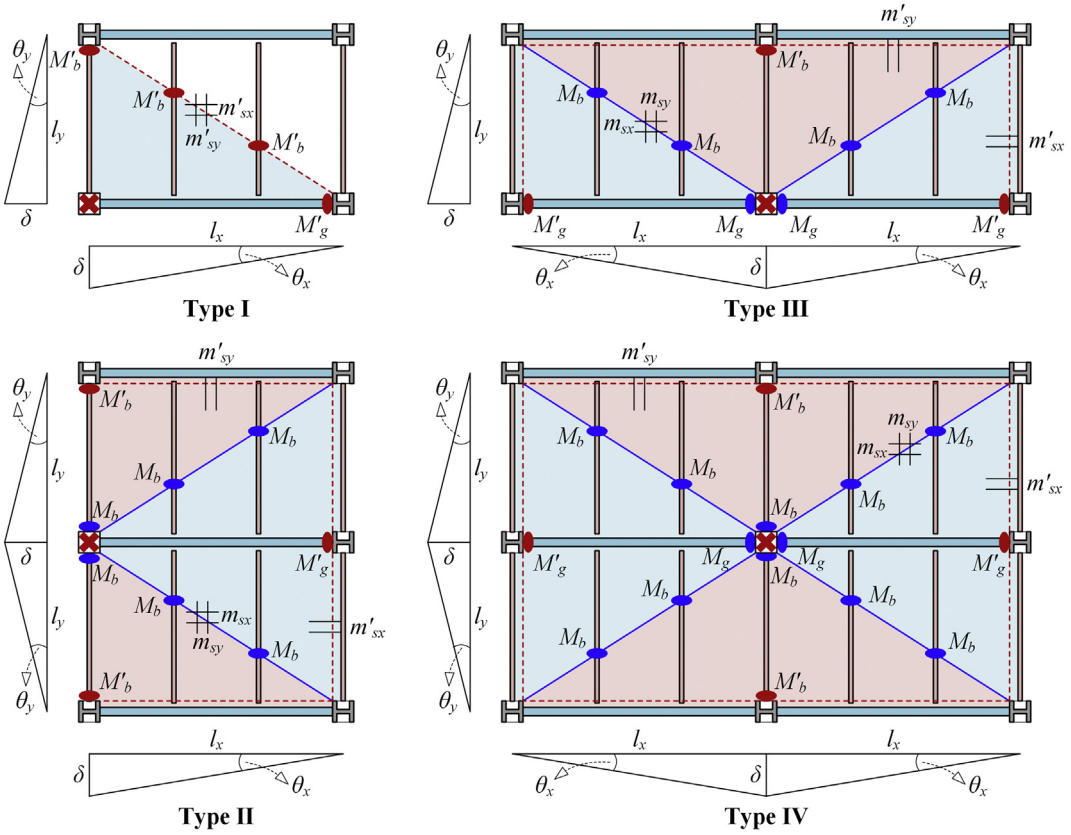

Type I	Type II	Type Ⅲ	Type IV
A1	A2, A3	B1, C1	B2, B3, C2, C3

Fig. 3. Yield-line configuration of composite floor system.

The external work $W_{external}$ corresponding to Type I is calculated according to Eq. 5; $W_{external}$ corresponding to Type II and Type III is calculated according to Eq. 6, and $W_{external}$ corresponding to Type IV is calculated according to Eq. 7.

$$W_{external} = \omega_y l_x l_y \delta/6 \tag{5}$$

$$W_{external} = 2\omega_y l_x l_y \delta/3 \tag{6}$$

$$W_{external} = 4\omega_y l_x l_y \delta/3 \tag{7}$$

Then, the ω_y corresponding to each column removal case can be obtained by Eq. 8.

$$W_{internal} = W_{external} \tag{8}$$

2.2. Plastic stage

Because the catenary action and the tension membrane action cannot be fully developed in the A1, A2, B1, and B2 cases, as shown in Fig. 2(a), it is assumed that the load-displacement curve of the theoretical model in these cases is a horizontal line after the displacement exceeds δ_y. Fu et al. [12] found that when the vertical displacement δ exceeds twice the height of the composite beam section, the resistance of the structure will decrease. Therefore, δ_u is defined as twice the section height of the composite beam.

For the A3, B3, C1, C2, C3 cases, as shown in Fig. 2(b), there are two stages after the elastic stage, namely the plastic stage and the catenary stage. These two stages are divided by the vertical displacement δ_t, where the sum of the resistance provided by the catenary action and the tensile membrane action exceeds the resistance provided by the flexural mechanism. Eq. (9) defines the load-displacement curve of these two stages.

$$\omega = \begin{cases} \omega_y \text{ (plastic stage)} \\ \omega_c + \omega_m \text{ (catenary stage)} \end{cases} \tag{9}$$

ω_c and ω_m represent the uniformly distributed load of the floor carried by the catenary action and the tensile membrane action, respectively.

2.3. Catenary stage

The resistance provided by the catenary action corresponding to the A3, B3, C1, C2 and C3 cases can be calculated according to Fig. 4. F_g is the tensile yield force provided by the residual section of the girder-to-column connection. F_b and F'_b are the tensile yield force provided by the residual section of the beam-to-column connection and beam-to-girder connection, respectively. For the welded flange-bolted web connection, F_g and F_b are the tensile yield force provided by the shear tab and the unbroken flange of the girder or beam. For the hinged beam-to-girder connection, F'_b is the tensile yield force provided by the shear tab. The catenary action provided by the A3, B3, C1, C2 and C3 cases can be calculated by Eqs. 10 to 14, respectively. It can be seen that the δ-ω_c curve is a straight line passing through the origin.

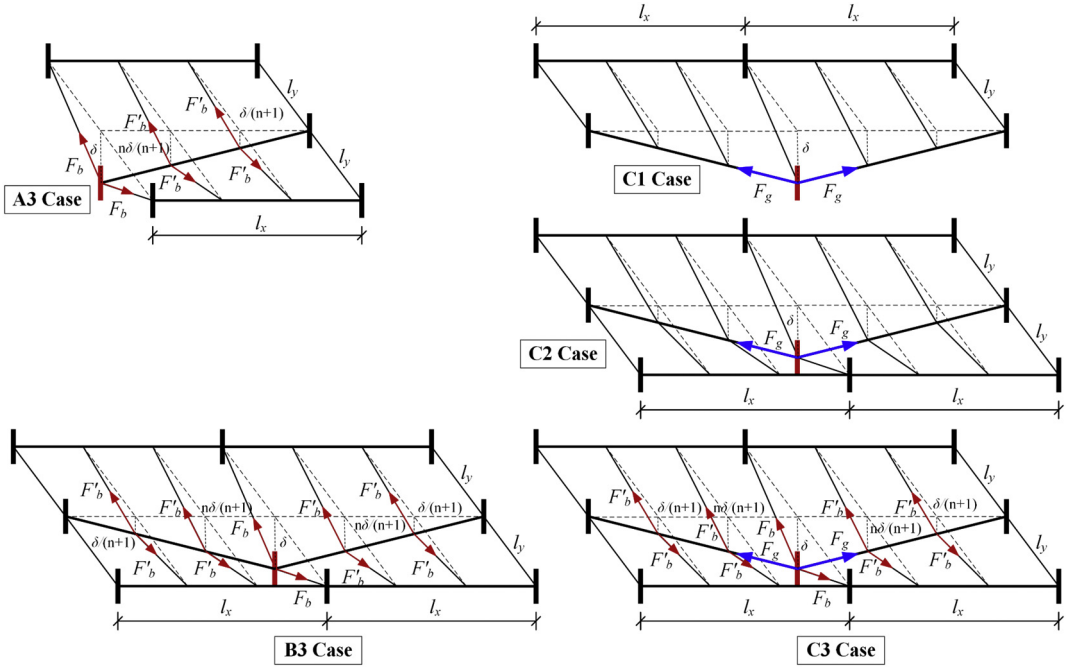

Fig. 4. Catenary action of beam system.

$$\text{A3 case } \omega_c = \frac{\frac{2F_b\delta}{l_y} + \frac{2F_b'\delta\left(\frac{n}{n+1}+\frac{n-1}{n+1}+\cdots+\frac{1}{n+1}\right)}{l_y}}{2l_xl_y} = \frac{\left(2F_b + nF_b'\right)\delta}{2l_xl_y^2} \quad (10)$$

$$\text{B3 case } \omega_c = \frac{\frac{2F_b\delta}{l_y} + \frac{4F_b'\delta\left(\frac{n}{n+1}+\frac{n-1}{n+1}+\cdots+\frac{1}{n+1}\right)}{l_y}}{4l_xl_y} = \frac{\left(F_b + nF_b'\right)\delta}{2l_xl_y^2} \quad (11)$$

$$\text{C1 case } \omega_c = \frac{\frac{2F_g\delta}{l_x}}{2l_xl_y} = \frac{F_g\delta}{l_x^2l_y} \quad (12)$$

$$\text{C2 case } \omega_c = \frac{\frac{2F_g\delta}{l_x}}{4l_xl_y} = \frac{F_g\delta}{2l_x^2l_y} \quad (13)$$

$$\text{C3 case } \omega_c = \frac{\frac{2F_g\delta}{l_x} + \frac{2F_b\delta}{l_y} + \frac{4F_b'\delta\left(\frac{n}{n+1}+\frac{n-1}{n+1}+\cdots+\frac{1}{n+1}\right)}{l_y}}{4l_xl_y} = \frac{F_g\delta}{2l_x^2l_y} + \frac{\left(F_b + nF_b'\right)\delta}{2l_xl_y^2} \quad (14)$$

As shown in Fig. 4, it can be seen that, among the five column removal cases, only the C3 case can simultaneously develop catenary force in both directions of girder and beam. Similarly, as depicted in Fig. 5(a), only the C3 case can develop the two-way membrane force, which calculation diagram is illustrated in Fig. 5(b). T_x and T_y are the tensile membrane forces developed by the per-unit width floor slab in the x and y directions, respectively. T_x and T_y are equal to the yield tensile force developed by the per-unit width slab reinforcement and steel deck in the respective directions. For the commonly used trapezoidal steel deck and re-entrant steel deck, it is assumed that the tensile membrane force only develops along the direction of the deck rib. Since the two ends of the steel deck are only connected to the upper flange of the steel beam by shear studs at the bottom of the deck rib, the tensile membrane force of the steel deck developed along the direction of the deck rib only considers the contribution of the bottom deck rib.

In Fig. 5, the uniform load carried by the unit area rectangular element with side lengths dx and dy is ω_m. The load balance formula of the floor slab in the normal direction (z direction) is

$$0 = \omega_m dxdy - T_x dy\frac{\partial z}{\partial x} + T_x dy\left(\frac{\partial z}{\partial x} + \frac{\partial^2 z}{\partial x^2}dx\right) - T_y dx\frac{\partial z}{\partial y} + T_y dx\left(\frac{\partial z}{\partial y} + \frac{\partial^2 z}{\partial y^2}dy\right) \quad (15)$$

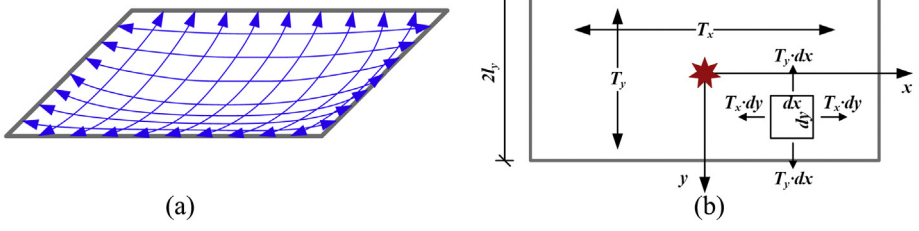

Fig. 5. Two-way tensile membrane action of C3 case.

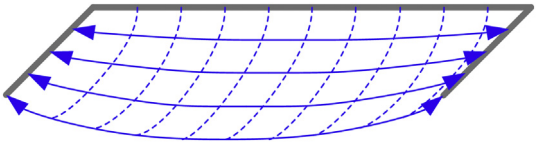

Fig. 6. One-way tensile membrane action of C1 case.

Then,

$$\frac{T_x}{T_y}\cdot\frac{\partial^2 z}{\partial x^2}+\frac{\partial^2 z}{\partial y^2}=-\frac{\omega_m}{T_y} \tag{16}$$

Replacing x in the above equation with X, Eq. 17 can be obtained.

$$X = x\cdot\sqrt{T_y/T_x} \tag{17}$$

Then, Eq. 16 can be converted into

$$\frac{\partial^2 z}{\partial X^2}+\frac{\partial^2 z}{\partial y^2}=-\frac{\omega_m}{T_y} \tag{18}$$

In Eq. 18, z at the boundary of the rectangular floor ($x=\pm l_x, y=\pm l_y$) is equal to 0. Then, according to Park et al. [16], Timoshenko et al. [17], the solution of Eq. 18 is

$$\frac{\omega_m l_y^2}{T_y\delta}=\frac{\pi^3}{4\sum_{n=1,3,5,\ldots}^{\infty}\frac{1}{n^3}(-1)^{\frac{n-1}{2}}\left\{1-\frac{1}{\cosh\left[\left(\frac{n\pi l_x}{2l_y}\right)\sqrt{T_y/T_x}\right]}\right\}}=C \tag{19}$$

where, C is a constant. Thus, ω_m can be obtained as

$$\omega_m = C\frac{T_y\delta}{l_y^2} \tag{20}$$

According to Eq. 20, it can be seen that the δ-ω_m curve is also a straight line passing through the origin.

For A3, B3, C1 and C2 cases, only one-way tensile membrane force can be developed. As shown in Fig. 6, taking C1 case as an example, eliminating the y term in Eq. 16 can obtain Eq. 21.

$$\frac{\partial^2 z}{\partial x^2}=-\frac{\omega_m}{T_x} \tag{21}$$

The solution of Eq. 21 is

$$\omega_m=\frac{2T_x\delta}{l_x^2} \tag{22}$$

The bearing capacity provided by the one-way tensile membrane action corresponding to the A3, B3, and C2 cases can also be derived in the same way.

In summary, the loads ω_c and ω_m carried by the catenary action and the tensile membrane action have been obtained, and the displacement δ_t can be obtained according to Eq. 23.

$$\omega_y=\omega_c+\omega_m \tag{23}$$

3. Comparisons with the experimental tests

Fig. 7 and Table 1 show the comparisons between the predicted results of the theoretical model and the test results of five frame structures with floor slabs. The five test specimens include: PE1 specimen (Dat et al. [18]), MD specimen (Qian et al. [19]), 2 × 3-S-PI specimen (Fu et al. [3]), 2G1B-IN specimen (Wang et al. [20]) and 2G1B-OUT specimen (Wang et al. [21]). Specimen PEI is a typical reinforced concrete floor structure composed of concrete beams and concrete floor slabs, while specimen MD is a concrete flat slab structure. The remaining three test specimens are steel frame structures with composite floor slabs. Among the five specimens, the 2G1B-IN specimen has a relatively strong horizontal boundary constraint so that it can develop significant catenary action and tensile membrane action at the large deformation stage. The remaining four specimens have weak horizontal boundary

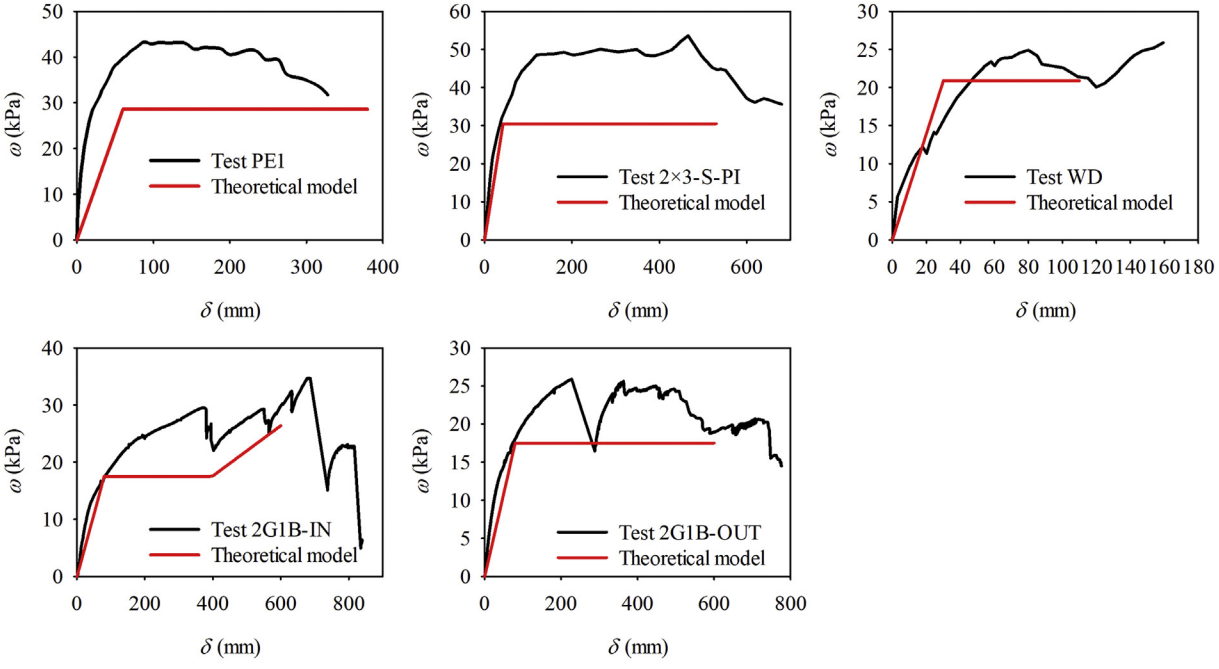

Fig. 7. Comparison of theoretical model and test results.

Table 1
Comparison with the experimental results.

Specimen	Structure type	Ultimate load (kPa)			Ultimate displacement (mm)		
		Test	Model	Model/Test	Test	Model	Model/Test
PE1	Concrete structure	43.1	28.6	0.66	330	390	1.18
WD	Concrete structure	25.9	20.9	0.81	159	110	0.69
2 × 3-S-PI	Composite structure	52.3	30.5	0.58	679	530	0.78
2G1B-OUT	Composite structure	25.6	17.5	0.68	748	600	0.80
2G1B-IN	Composite structure	34.6	26.4	0.76	816	600	0.74

constraints, so in the theoretical calculation, only the contribution of the flexural mechanism is considered.

Based on the comparison of the results in Fig. 7 and Table 1, it can be seen that, except for the 2 × 3-S-PI specimen, the other four specimens' ultimate theoretical resistance is 0.66–0.81 of its corresponding experimental value. However, this ratio of the 2 × 3-S-PI specimen is only 0.58. This is because the beam span of the 2 × 3-S-PI specimen is only 2 m, while the span-to-height ratio of the composite beam is only 7.4, which is much smaller than the common range of 10–20 for steel structural beams. This relatively smaller span-to-height ratio induces a larger arch resistance in composite beams, resulting in the test value being much higher than the theoretical prediction value. Besides, as the theoretical model uses the yield strength of steel to calculate, it does not consider the beneficial contribution of steel strain hardening, which will also cause the predicted value of the theoretical model lower than the experimental value. For the specimen 2G1B-IN, the theoretical model curve is closer to the experimental curve in the catenary stage, but the final displacement selected by the model is conservative, making the predicted ultimate resistance capacity lower. Although this theoretical model's prediction value is relatively rough, as its simplicity and ease of use, it can be used to make a conservative preliminary estimate of the progressive collapse resistance of the floor system at the design stage.

Except for the specimen PE1, the other four specimens' theoretical failure displacement is 0.69–0.80 of the experimentally measured displacement when the resistance capacity is losing. For the PE1 specimen, the ratio of the theoretically predicted failure displacement to the corresponding measured displacement is 1.18. This is because the deformation space available for the PE1 specimen is not enough, so the experiment is terminated prematurely. If there is sufficient deformation space for the PE1 specimen, its load-displacement curve should be able to develop to a larger displacement.

In addition to comparing the experimental results, in the following section, the theoretical model is also compared with the numerical simulation results.

4. Comparisons with finite element simulations

4.1. Prototype buildings

Fig. 8 (a) depicts two 5-story prototype steel frame buildings (Building A, Building B) designed according to Chinese codes [22,23]. The seismic design intensity of Building A and Building B is VI, which corresponding design basic earthquake acceleration is 0.05 g (gravitational acceleration). The design dead load (DL) is 5 kN/m^2, and the live load (LL) is 2 kN/m^2. The girder spans for Building A and Building B are 9 m and 6 m, respectively. The beam span, beam spacing, and each floor's height for these two buildings are identical, which is 6 m, 3 m, and 4.5 m, respectively. Except for the girder and the column, all the structural member sizes and material properties of these two buildings are the same. The H-section girder selected for Building A and Building B is H500 × 200 × 10 × 16 and H300 × 150 × 6.5 × 9, respectively. The nomenclature of the H-section beam is as follows: H (beam height) × (flange width) × (web thickness) × (flange thickness). The square steel column selected for Building A and Building B is □400 × 400 × 12 (width is 400 mm, wall thickness is 12 mm) and □350 × 350 × 10, respectively. The section size of the H-shaped steel beam is H300 × 150 × 6.5 × 9. As shown in Fig. 8 (b) and 8 (c), all the girder-to-column connections and beam-to-column connections are designed as welded flange-bolted web connection, while the beam-to-girder connections are designed as shear tab connection. As shown in Fig. 8 (d), A 100 mm thick composite slab is selected to support the designed gravity load. The 1.2 mm trapezoidal steel deck is parallel to the girder. The slab reinforcement is steel mesh fabricated with 8 mm diameter rebars, which spacing in both directions is 200 mm. The girder/beam and composite slab are connected by 19 mm diameter shear studs, which quantities on the 9 m and 6 m span girders are 85 and 55, respectively. Each beam has 38 shear studs. Full shear connection is achieved both in girders and beams, so, the shear failure of the shear studs is not considered in the macro model of the prototype buildings. Considering the 100 mm thick composite slab above the girder and beam, the span-to-depth ratios of the composite girder and composite beam in these two buildings are 15. The material properties of the steel decks, reinforcement steel, shear studs and concrete used in these prototype buildings are shown in Fig. 8 (e). The steel properties used for the girders, beams, and columns are identical to those used in the girder flanges of the test specimen conducted by Wang et al. [24]. The cylindrical compressive strength of concrete is 26 MPa.

4.2. Modeling approaches

This section presents the modeling approach for the macro model of steel frame building, which is implemented using the LS-DYNA software.

4.2.1. Girder(beam)-to-column connection

Fig. 9(a) shows a close up of the modeling approach of the composite floor neighboring to the connection region. All the girders, beams, and columns are modeled by the Hughes-Liu beam element with cross-section integration. The welded girder flange and bolted web in the connection region is modeled by discrete beam elements, which is using a general spring material model (material 119 in LS-DYNA). To ensure an appropriate failure mode, these connection springs are only permitted to fail along its axial direction. The axial load-deformation relationship is represented by the trilinear model depicted in Fig. 9(b). For the welded flange-bolted web connection, the welded flanges and bolt connections failure are caused by tension rather than compression [25,26]. Hence, the trilinear model in Fig. 9(b) only decreases after reaching its ultimate tensile resistance (t_u), and no drop is assumed after reaching its ultimate compressive resistance ($-t_u$).

The fracture behavior of the girder(beam)-to-column connections is highly influenced by the stress state. The steel fracture loci, considering the effect of stress triaxiality and Lode angle, are selected the fracture model used by Wang et al. [24], which is calibrated using the girder flanges used in that study. However, these fracture loci can only be directly used for the solid element model, as the stress state can only be accurately obtained from this model. Hence, an indirect approach is used here: the connection springs will be calibrated with corresponding

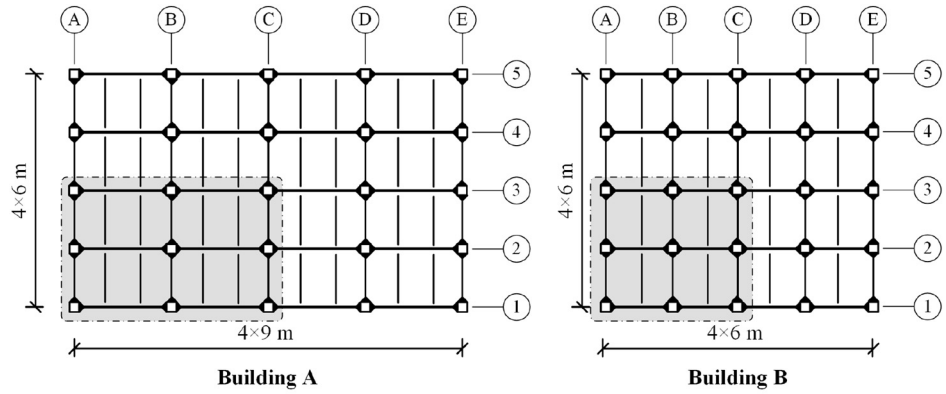

(a) Plan view

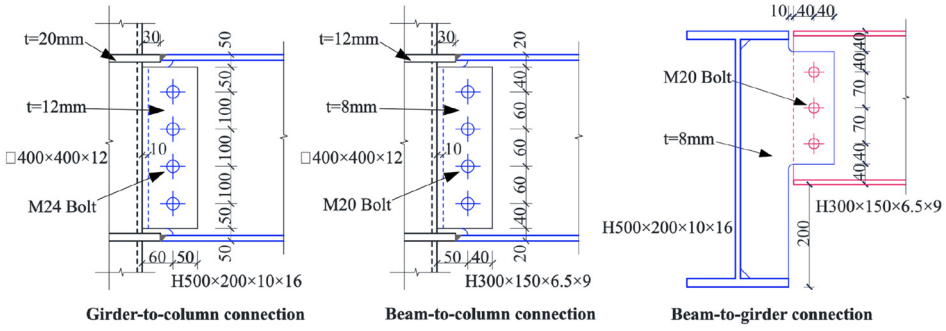

(b) Connection details of Building A

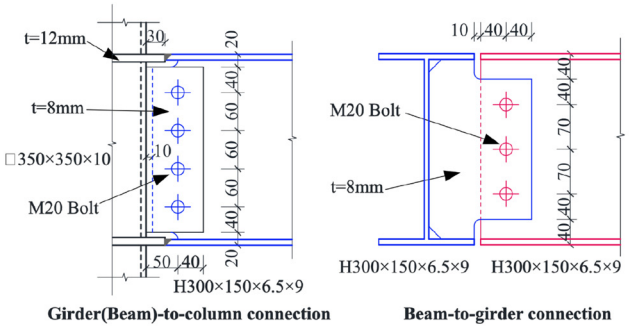

(c) Connection details of Building B

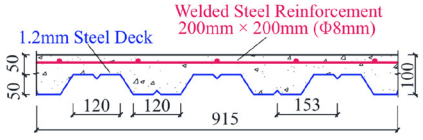

(d) Composite slab

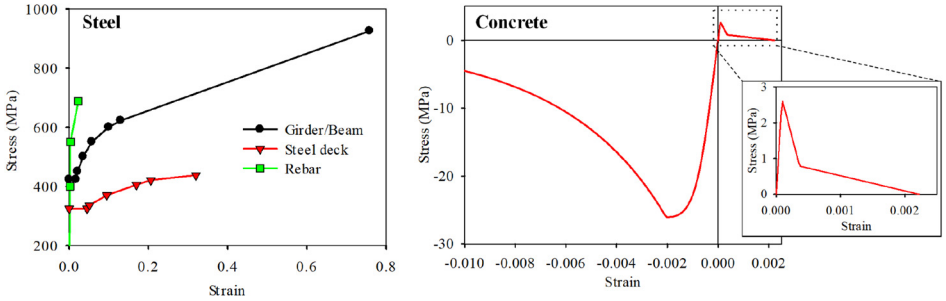

(e) Material properties

Fig. 8. Prototype buildings.

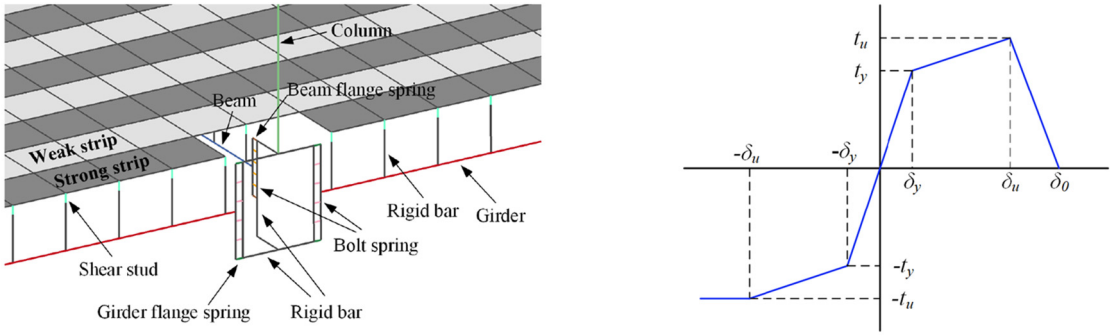

(a) Modeling approach of the connection region (b) Axial load-deformation relationship for connection spring

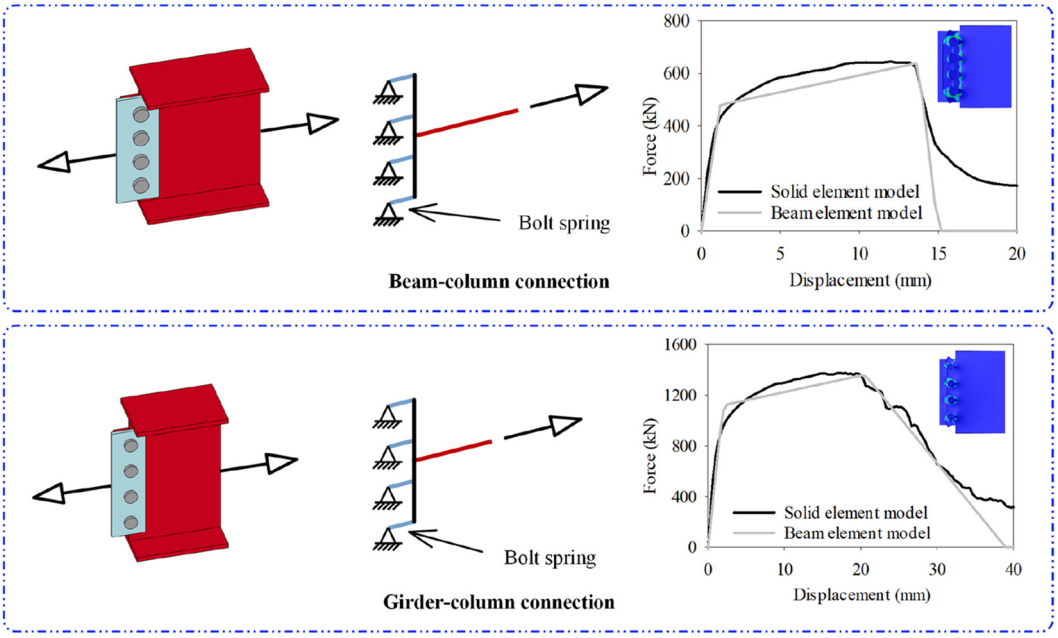

(c) Bolt spring calibration

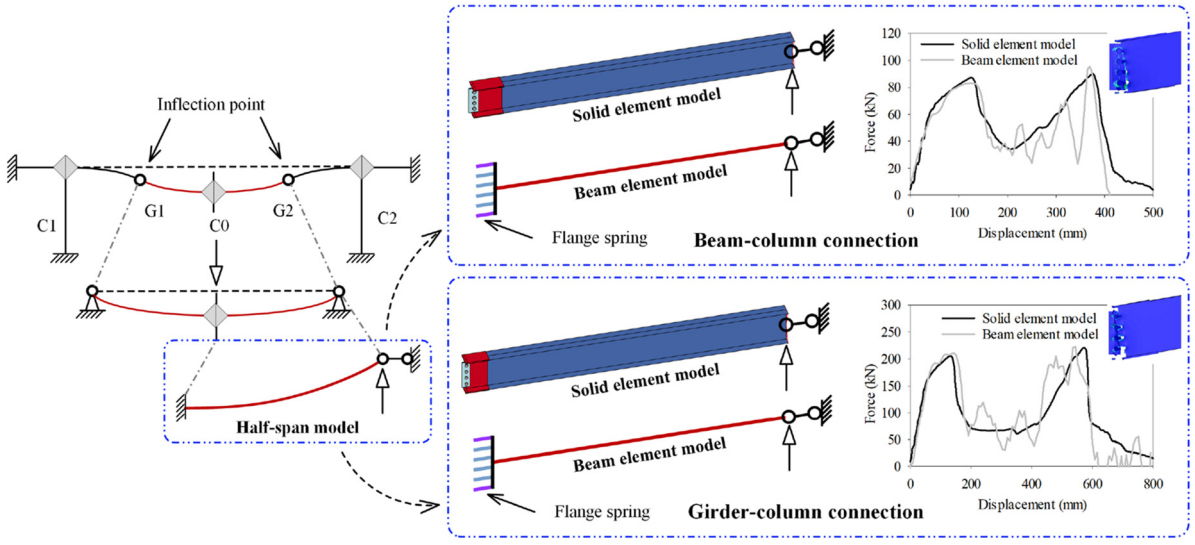

(d) Flange spring calibration

Fig. 9. Macro model of the connection region.

Table 2
Calibrated connection spring parameters for Building A.

Connection	Spring	δ_y (mm)	t_y (kN)	δ_u (mm)	t_u (kN)	δ_0 (mm)
Girder-to-column	Bolt spring	1.5	280	20	340	39
	Flange spring	0.02	1354	2.05	1818	2.55
Beam-to-column	Bolt spring	1	125	13.5	160	16
	Flange spring	0.02	571	2	760	2.5

connections modeled with solid elements. Fig. 9 (c) depicts the bolt spring's calibration procedure, which are calibrated with two bolted web connection models extracted from the girder(beam)-to-column connection of Building A. Displacement controlled tensile loading is applied to these bolted web connection models along its axial direction. After several iterations, the bolt spring's parameters are obtained when the beam element model's result matches the solid element model, as shown in Fig. 9 (c).

As depicted in Fig. 9 (d), the behavior of the girder(beam)-to-column connection under column loss scenario can be simplified and represented by a half-span model [24]. Both the solid element model and beam element model for Building A are established here. The calibrated bolt springs mentioned above are used to these beam element half-span models. Similarly, the flange spring's parament is calibrated when these two model's results fit well with each other (Fig. 9 (d)). Because the material properties and bolt connection dimensions are identical for both the beam-to-column connection and beam-to-girder connection, the bolt spring calibrated for the beam-to-column connection is applied to the beam-to-girder connection in the macro model. Table 2 lists the calibrated connection springs' parameters for Building A. The same connections are also used in Building B.

4.2.2. Composite floor slab

Fig. 10(a) depicts the modeling approach for the composite slab's macro model. To reduce computational time and resources, the composite slab is modeled by 300 × 300 mm shell elements with through-thickness integration. Due to the cross-section shape's variation of the composite slab, the shell elements are classified into two types, as denoted by strong strip and weak strip in Fig. 9(a) and Fig. 10(a). Strong strip represents the 100 mm thick slab section with flange and rib, while the weak strip represents the 50 mm thick slab section only composed of the flange. Strong strips have seven integration points, including four concrete points, two slab reinforcement points, and one steel deck point. Given that the steel deck is only constrained at its bottom surface by the shear stud, the steel deck is not considered in the weak strip, which is composed of six integration points. In order to ensure the model's continuity, the strong strip element nodes are located at the mid-thickness of the shell, while the weak strip element nodes are located at the bottom surface of the shell.

The performances of concrete, slab reinforcement and steel deck in the shell element are characterized by the material 172 in LS-DYNA. By altering the percentage of reinforcement, this material model can represent both concrete and smeared reinforcement, or a combination of them. The stress-strain curves used in this material model are illustrated in Fig. 8 (e). To avoiding the mutual influence between the steel reinforcements in two directions, as shown in Fig. 10(a), they are modeled by two separate integration nodes. Therefore, the reinforcement failure in one direction will not result in premature reinforcement failure in the other direction. Since the steel deck in the direction perpendicular to the slab rib is curled, it can not develop tensile resistance in this direction. Hence, the material property of the steel deck integration point is only defined in the direction parallel to the slab rib. In the case of convergence problem and too large unrealistic element

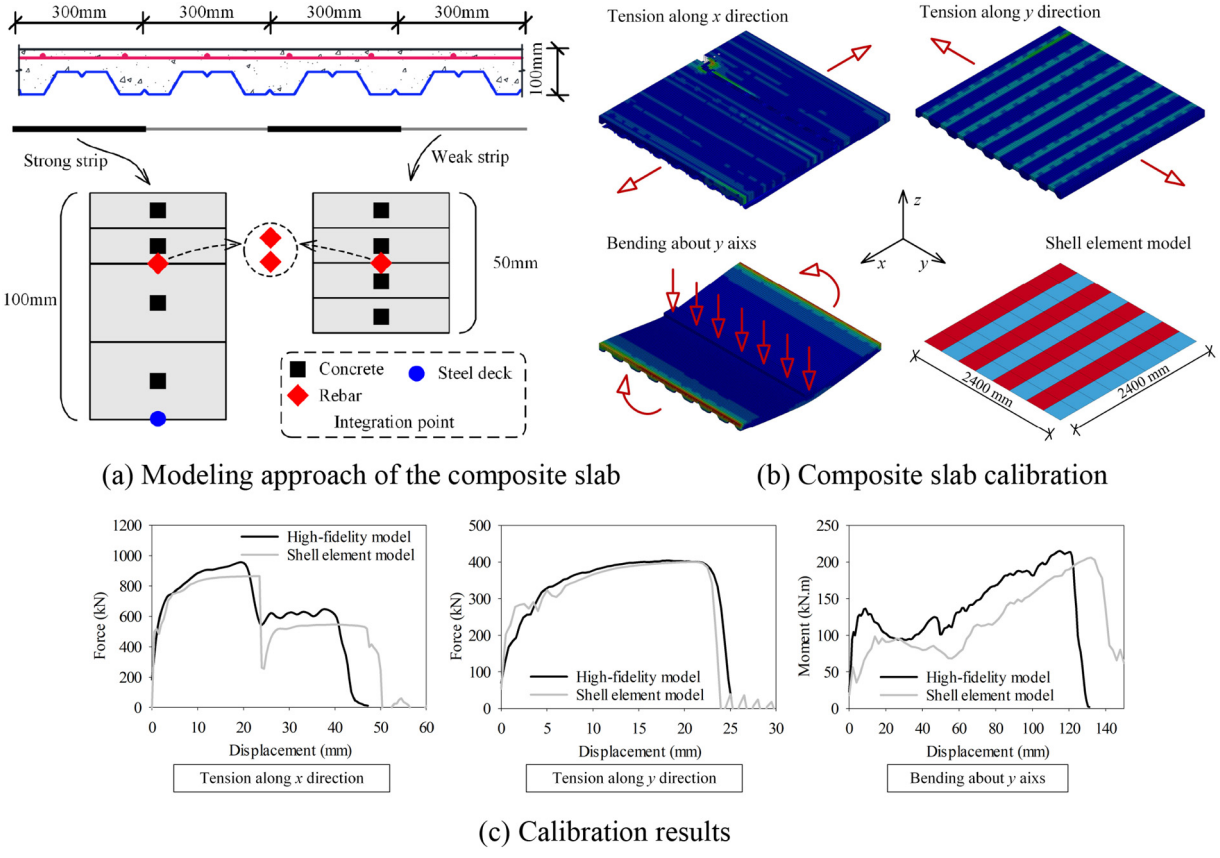

Fig. 10. Macro model of the composite slab.

distortion, the shell elements of both strong strip and weak strip are deleted from the model when its plastic strain reaches 0.3.

Under the progressive collapse scenario, the primary contributions of the composite slab are the bending resistance and the spatial tensile membrane action. Limited by the inherent cross-section property, the composite slab with trapezoidal steel deck used in this study is performed as a one-way slab, therefore, as shown in Fig. 10(b), it can only resist bending load about the y axis (perpendicular to the slab rib). However, it can develop tensile force both along x direction (parallel to the slab rib) and y direction. Both the steel deck and slab reinforcement contribute to the developed tensile force along x direction, while the tensile force along y direction is only developed by the slab reinforcement. Fig. 10(b) describes the calibration routine: at first, a 2400 × 2400 mm square composite slab is extracted from the test specimen, and corresponding high-fidelity model is established following the modeling procedure described by Wang et al. [24]; the next step is to analyze the tensile response along x direction and y direction, and the flexural behavior about y axis; at last, altering the material properties of the shell element model to make its results consistent with those obtained from the high-fidelity model. It is worth noting that, for steel deck in the high-fidelity model, only bottom element nodes are applied with tensile force (tension along x direction case) or horizontal constraint (bending about y axis), which is in keeping with the actual boundary conditions in currently designed steel buildings. Fig. 10(c) presents the comparison between the calibrated shell element model and the high-fidelity model, which indicates this shell element model is applicable to the progressive collapse analysis of the composite slab. The element number of the high-fidelity model and shell element model is 41,088 and 64, respectively. Hence, the computational cost is notably reduced.

4.2.3. Other modeling approaches

Fig. 9(a) depicts the modeling method of shear stud: Rigid bars extend from the girder/beam nodes to their top flange, and discrete beam elements are utilized to connect these rigid bars to the composite slab. The yield stress, ultimate stress and ultimate strain of shear stud is assumed as 320 MPa, 400 MPa and 0.14, respectively. In the pushdown analysis of the overall structure, the failed column is removed before the uniform vertical load is applied. On the floor slabs affected by the removed column and the floor slabs above it, gradually increasing vertical load is uniformly applied until the entire structure reaches its ultimate load-carrying capacity. The affected area of the removed column is defined according to ASCE/SEI 7–16 [27]. Except for the removed column, all other columns are fixed at their bases. The total vertical reaction at the column bases is regarded as the building resistance, and load intensity is calculated by dividing the building resistance by the floor area subjected to pushdown loading. Hence, the relationship between the load intensity and the vertical displacement at the removed column is thus obtained.

4.3. Simulation results and comparison with theoretical model

Fig. 11 shows the load intensity-displacement curves of the prototype buildings at each column removal scenario. Fig. 12 shows the vertical displacement contours of prototype buildings. Table 3 summarizes the ultimate resistance of the Building A (R_A) and Building B (R_B) under

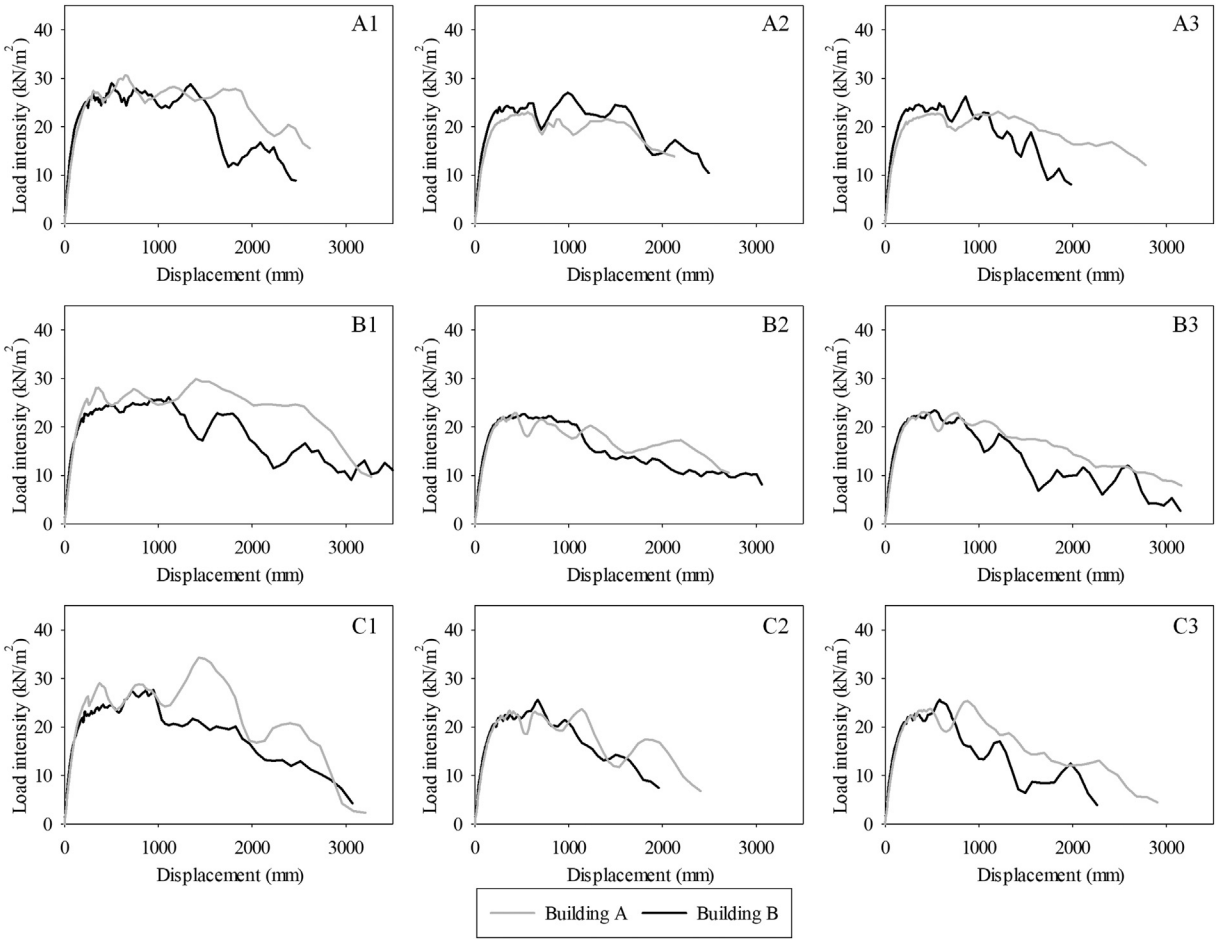

Fig. 11. Simulated load-displacement results of Building A and Building B.

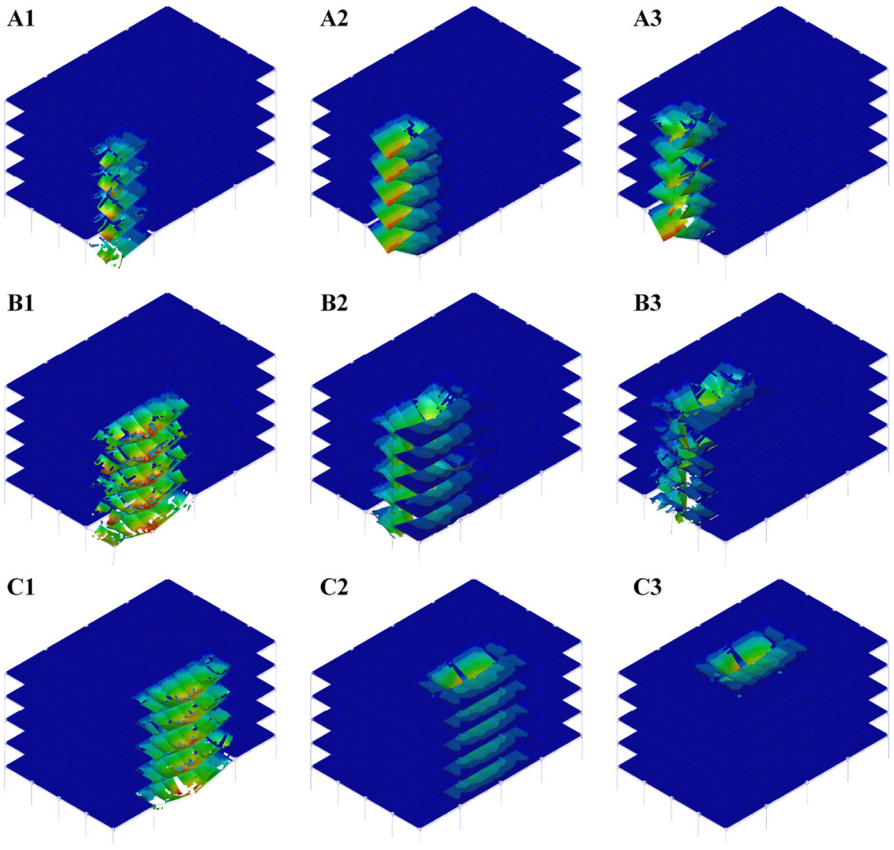

(a) Building A

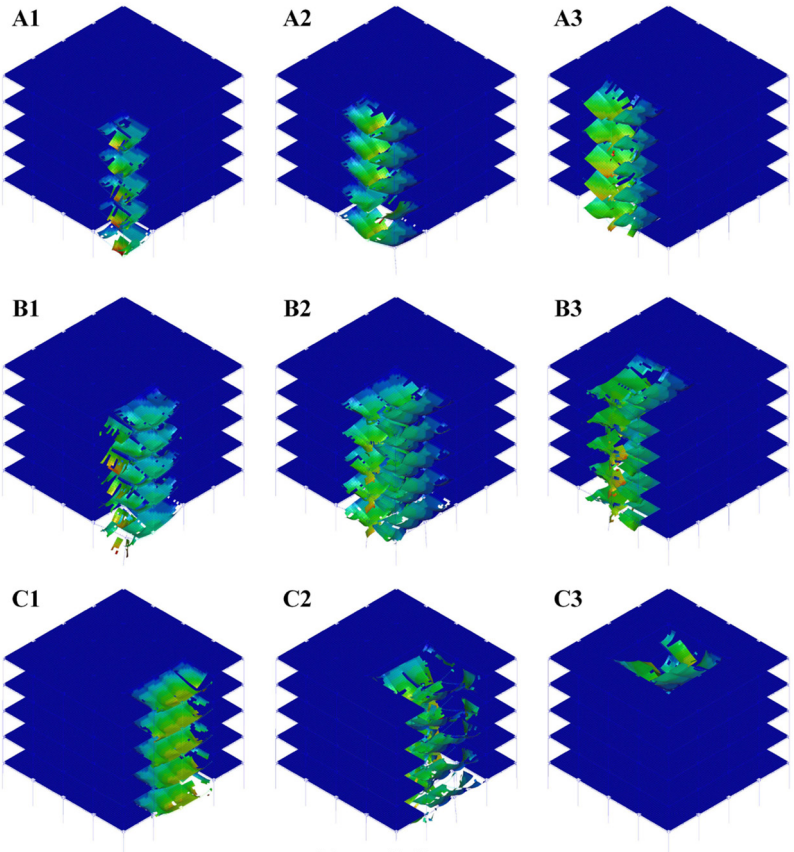

(b) Building B

Fig. 12. Vertical displacement contours of prototype buildings.

Table 3
Ultimate resistance of Building A and Building B.

Removed column	1.2DL + 0.5LL	Building A		Building B		
	R_d (kN/m^2)	R_A (kN/m^2)	R_A/R_d	R_B (kN/m^2)	R_B/R_A	R_B/R_d
A1	7	30.61	4.37	28.99	0.95	4.14
A2	7	23.07	3.30	27.05	1.17	3.86
A3	7	23.12	3.30	26.24	1.14	3.75
B1	7	29.88	4.27	26.10	0.87	3.73
B2	7	22.87	3.27	22.62	0.99	3.23
B3	7	23.11	3.30	23.42	1.01	3.35
C1	7	34.29	4.90	27.63	0.81	3.95
C2	7	23.70	3.39	25.57	1.08	3.65
C3	7	25.36	3.62	25.62	1.01	3.66

each column removal scenario, and compares it with the load combination for extraordinary events R_d (1.2 DL + 0.5 LL = 7 kN/m^2) specified in ASCE/SEI 7–16 [27].

As shown in Table 3, for all column failure cases, R_A far exceeds its corresponding R_d. C1 case has the highest R_A, which is 4.90 times of R_d, and the R_A of the B2 case is the lowest, which is 3.27 times of R_d. These indicate that Building A can successfully prevent the progressive collapse caused by the removal of a single ground floor column. The R_A of A1, B1, and C1 cases is at least 4.27 times of R_d, while the R_A of the other six cases excluding the C3 case is about 3.3 times that of R_d. Compared with the other six cases, the higher R_A of the A1, B1 and C1 cases is benefiting from the relatively smaller tributary floor area of the affected girders, which is only half of the girder's tributary floor area of other six cases. Except for the A1, B1, and C1 cases, the R_A of the C3 case is slightly higher than the other cases, which is owing to the development of two-way tensile membrane action after the surrounding horizontal boundaries are constrained. For the B2 and B3 cases, the load intensity-displacement curves exhibit an obvious downward trend after reaching their maximum flexural resistance, which indicates the catenary action and tensile membrane action cannot be fully developed at the large deformation stage due to the weak horizontal constraints.

After reducing the girder span from 9 m to 6 m, the most vulnerable case is still B2, but its R_B is still much greater than R_d, that is 3.23 times larger. For these two buildings, relatively higher resistance is achieved when girder side columns (B1 and C1) or corner column (A1) fails, while the internal column (B2, B3, C2, and C3) or beam side column (A2 and A3) failure cases are relatively vulnerable. In addition, the ultimate resistance of these three buildings is at least 3.23 times of R_d., which indicates these buildings have a superior progressive collapse resistance. The excellent performance of the steel frame buildings with

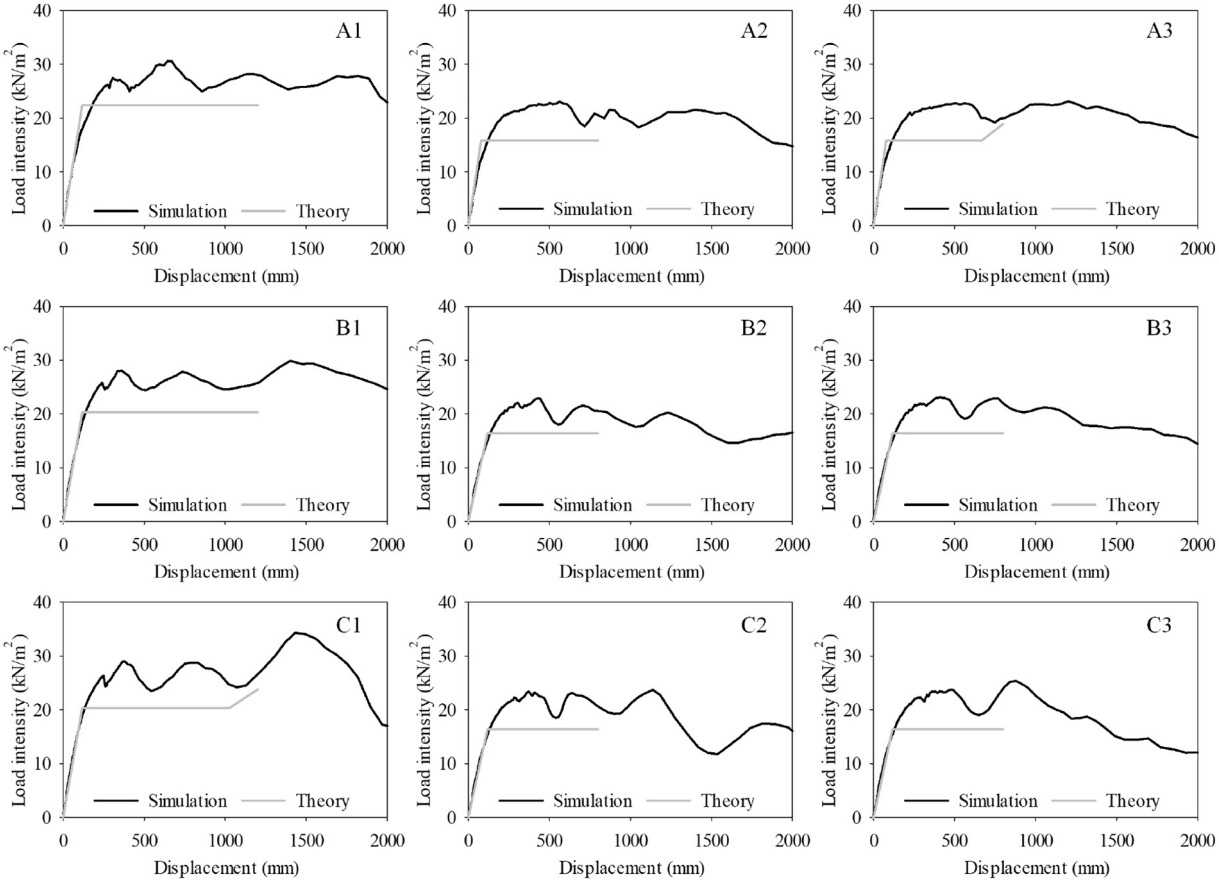

(a) Building A

Fig. 13. Comparison between theoretical model and simulation results.

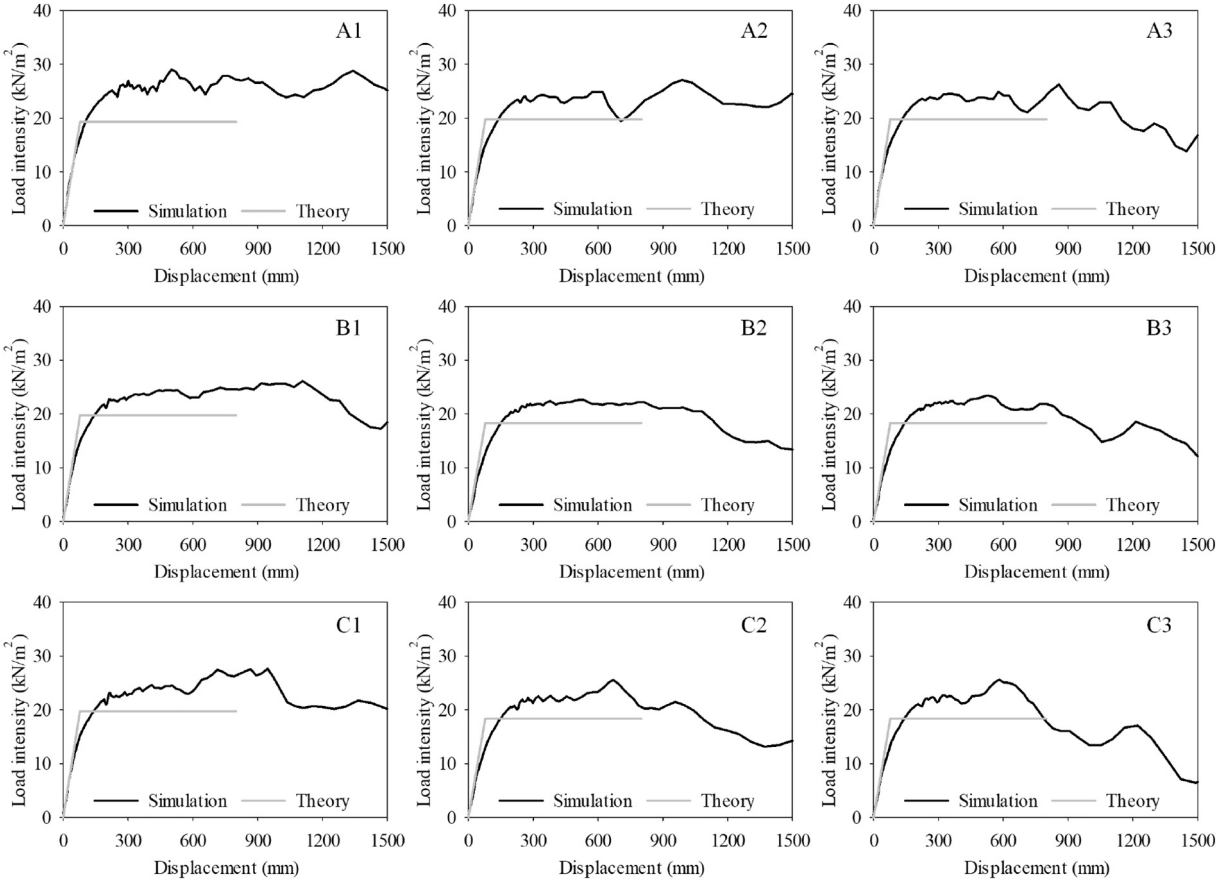

(b) Building B

Fig. 13 (*continued*).

composite slab against column loss is owing to the current design method. In the seismic design of steel frame buildings, the composite slab's contribution to the flexural capacity of the girder/beam is neglected, which will significantly improve the structural resistance against progressive collapse.

Fig. 13 shows the comparison of the theoretical prediction of each column removal condition of the prototype buildings with the load-displacement curve of the numerical simulation results. It can be seen that the theoretically predicted ultimate resistance are close to the numerical simulation results. Therefore, this theoretical method is suitable to give a conservative preliminary estimate of the progressive collapse resistance of the steel frame buildings with composite slab at the design stage.

5. Model limitations

Although the theoretical method proposed in this paper is easy-to-use, it still has several limitations in predicting the actual progressive collapse resistance of steel frame buildings. First, the strain hardening effect is not considered for the structural steels, such as beams, slab reinforcement, and steel deck. Instead, all the structural steels are assumed to be perfect plasticity. Based on the structural steels used by Wang et al. [20], this simplification may underestimate the strength of the beam, slab reinforcement, and steel deck by 27%, 16%, and 11%, respectively. As this method aims to evaluate the progressive collapse resistance at the design stage, the steel yield strength is selected here for conservative purposes. Second, the compressive membrane action of the slab is not considered. The compressive membrane action development is highly affected by the boundary conditions and the span-depth ratio of concrete slab. Usually, the concrete slab used in the composite floor system is thinner than that of the reinforced concrete floor system, and can not develop obvious compressive membrane action. Hence, it is reasonable to neglect the contribution of compressive membrane action. However, if the span-depth ratio of concrete slab is too small, as the 2 × 3-S-PI specimen mentioned in Section 3, the neglect of compressive membrane action would be unacceptable. Third, δ_u used in this theoretical method is a empiric value, which needs to be verified by adequate experimental or numerical results. Despite these limitations, this theoretical method proposed in this paper can conveniently evaluate the progressive collapse resistance of steel frame buildings by hand calculation at the design stage, and give a conservative estimate.

6. Maximum tributary area of column

Different from the single-story structure, under the column removal scenario, the bottom column adjacent to the failed column in the multi-story or even high-rise steel frame structure will be subjected to significantly redistributed load, which is likely to cause the instability of the column. In Section 4.3, the failure of C2 and C3 cases of Building A are caused by the instability of the column. This phenomenon may be more serious in high-rise buildings. Bao et al. [28] simulated a 10-story reinforced concrete frame building, due to the instability of column under redistributed load, the collapse resistance of this 10-story building after sudden removal of column is only half that of the single-story structure. Therefore, the results predicted by the single-story structure may overestimate the collapse resistance of the

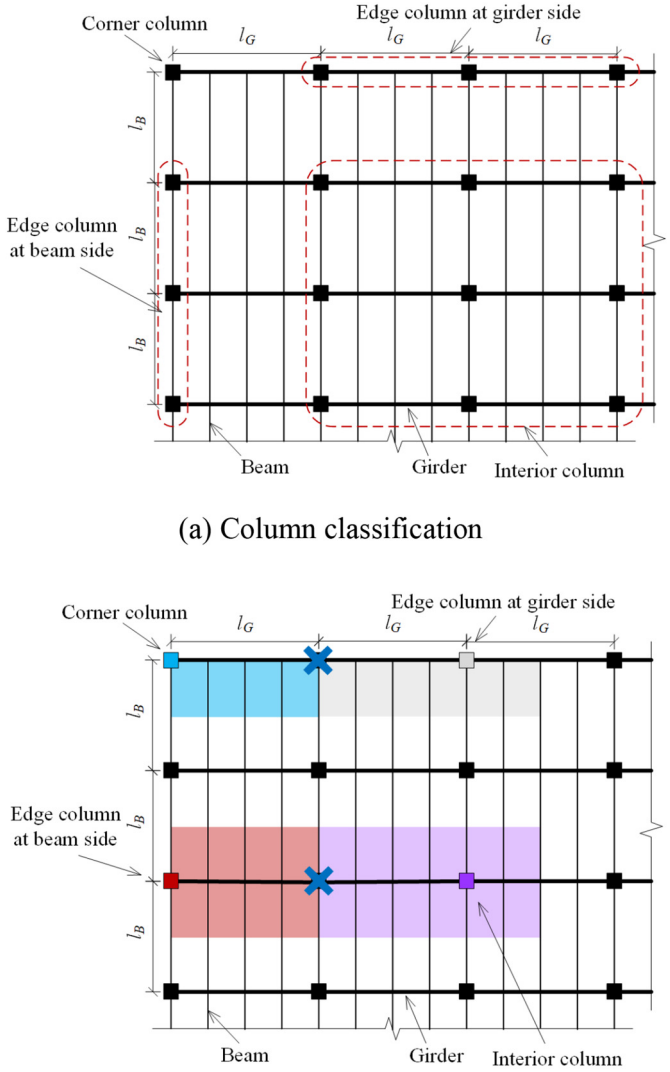

Fig. 14. Maximum tributary area of each column removal scenario.

multi-story or high-rise structure, and the effect of the redistributed load to the adjacent column should be considered. Hence, when conducting progressive collapse design, the vertical bearing capacity of bottom columns should be sufficient to bear the redistributed gravity load. For the regular structure shown in Fig. 14(a), the columns can be classified into four categories: corner column, edge column at girder side, edge column at beam side, and interior column. In Fig. 14(a), l_G represents the span of the girder, and l_B represents the span of the beam. Under the column removal scenarios, the maximum tributary area of each type column is illustrated as the shaded area in Fig. 14(b). The maximum tributary area of corner column, edge column at girder side, edge column at beam side, and interior column is $0.5l_Gl_B$, $0.75l_Gl_B$, l_Gl_B and $1.5l_Gl_B$, respectively. Therefore, at the structural design stage, the vertical bearing capacity of these columns must be able to bear the sum of the vertical loads of each upper floor within the maximum tributary area.

7. Conclusions

In this paper, an easy-to-use theoretical method is proposed to assess the progressive collapse resistance of steel frame structures with composite slab. This method, which is based on the yield line theory and membrane action theory, can give a reasonable and conservative prediction of the collapse resistance. With this theoretical method, most of the single column removal scenarios can be conveniently analyzed. When the floor system has been horizontally constrained at the parallel boundaries, the theoretical model is composed of three stages, i.e., elastic stage, plastic stage, and catenary stage. At the elastic stage and plastic stage, the load is carried by the flexural resistance of the beam system and the slab system, while at the catenary stage, the load is resisted by the catenary action and the tensile membrane action. When the floor system has been fully constrained at the horizontal boundary, the theoretical model is only composed of elastic stage and plastic stage. The model has been compared with the experimental and simulation results, where it demonstrates good capability to predict the progressive collapse resistance. Finally, for multi-story and high-rise buildings, considering the potential instability of columns under excessively redistributed gravity load, the potentially maximum tributary area of column under the progressive collapse scenario is presented.

Authorship statement

All persons who meet authorship criteria are listed as authors, and all authors certify that they have participated sufficiently in the work to take public responsibility for the content, including participation in the concept, design, analysis, writing, or revision of the manuscript. Furthermore, each author certifies that this material or similar material has not been and will not be submitted to or published in any other publication before its appearance in the *Journal of Constructional Steel Research*.

Declaration of Competing Interest

The authors declare that they have no known competing financial interests or personal relationships that could have appeared to influence the work reported in this paper.

Acknowledgments

The research presented in this paper was sponsored by the State Key Laboratory of Disaster Reduction in Civil Engineering (Tongji University) through Grant Nos. SLDRCE19-A-03 and Natural Science Foundation of China (NSFC) through Grant Nos. 52078366 and 51778459. Supports for this study were also provided by the Sustainable Structural Engineering Research Funds from Tongji Architectural Design (Group) Co. Ltd.

All persons who have made substantial contributions to the work reported in the manuscript (e.g., technical help, writing and editing assistance, general support), but who do not meet the criteria for authorship, are named in the Acknowledgements and have given us their written permission to be named. If we have not included an Acknowledgements, then that indicates that we have not received substantial contributions from non-authors.

References

[1] E.S. Johnson, J.E. Meissner, L.A. Fahnestock, Experimental behavior of a half-scale steel concrete composite floor system subjected to column removal scenarios, J. Struct. Eng. 142 (2) (2015), 04015133, .

[2] M. Hadjioannou, S. Donahue, E.B. Williamson, et al., Large-scale experimental tests of composite steel floor systems subjected to column loss scenarios, J. Struct. Eng. 144 (2) (2017), 04017184, .

[3] Q.N. Fu, K.H. Tan, X.H. Zhou, et al., Three-dimensional composite floor systems under column-removal scenarios, J. Struct. Eng. 144 (10) (2018), 04018196, .

[4] R. Zandonini, N. Baldassino, F. Freddi, et al., Steel-concrete frames under the column loss scenario: an experimental study, J. Constr. Steel Res. 162 (2019) 105527.

[5] F. Sadek, S. El-Tawil, H.S. Lew, Robustness of composite floor systems with shear connections: modeling, simulation, and evaluation, J. Struct. Eng. 134 (11) (2008) 1717–1725.

[6] Y. Alashker, S. El-Tawil, F. Sadek, Progressive collapse resistance of steel-concrete composite floors, J. Struct. Eng. 136 (10) (2010) 1187–1196.
[7] Y. Alashker, H. Li, S. El-Tawil, Approximations in progressive collapse modeling, J. Struct. Eng. 137 (9) (2011) 914–924.
[8] H. Li, S. El-Tawil, Three-dimensional effects and collapse resistance mechanisms in steel frame buildings, J. Struct. Eng. 140 (8) (2014), A4014017, .
[9] S. Jeyarajan, J.Y.R. Liew, Robustness analysis of 3D composite buildings with semi-rigid joints and floor slab, Structures 6 (2016) 20–29.
[10] C.G. Bailey, Membrane action of unrestrained lightly reinforced concrete slabs at large displacements, Eng. Struct. 23 (5) (2001) 470–483.
[11] Y. Alashker, S. El-Tawil, A design-oriented model for the collapse resistance of composite floors subjected to column loss, J. Constr. Steel Res. 67 (1) (2011) 84–92.
[12] Q.N. Fu, K.H. Tan, X.H. Zhou, et al., A mechanical model of composite floor systems under an internal column removal scenario, Eng. Struct. 175 (2018) 50–62.
[13] G.Q. Li, J.Z. Zhang, J. Jiang, Analytical modeling on collapse resistance of steel beam-concrete slab composite substructures subjected to side column loss, Eng. Struct. 169 (2018) 238–255.
[14] J.Z. Zhang, G.Q. Li, Collapse resistance of steel beam-concrete slab composite substructures subjected to middle column loss, J. Constr. Steel Res. 145 (2018) 471–488.
[15] C.E.N. Eurocode, 8: Design of Structures for Earthquake Resistance, Part 3: Assessment and Retrofitting for Buildings, European Committee for Standardization, Brussels, 2010.
[16] R. Park, W.L. Gamble, Reinforced Concrete Slabs, John Wiley & Sons, 1999.
[17] S.P. Timoshenko, J. Goodier, Theory of elasticity, McGraw-Hill1951.
[18] P.X. Dat, K.H. Tan, Experimental response of beam-slab substructures subject to penultimate-external column removal, J. Struct. Eng. 141 (7) (2015), 04014170, .
[19] K. Qian, B. Li, Load-resisting mechanism to mitigate progressive collapse of flat slab structures, Mag. Concr. Res. 67 (7) (2015) 349–363.
[20] J. Wang, W. Wang, Y. Bao, Full-scale test of a steel–concrete composite floor system with moment-resisting connections under a middle-edge column removal scenario, J. Struct. Eng. 146 (5) (2020), 04020067, .
[21] J. Wang, W. Wang, Y. Bao, et al., Full-scale test of a steel moment-resisting frame with composite floor under a penultimate edge column removal scenario, J. Constr. Steel Res. 162 (2019) 105717.
[22] Ministry of Housing and Urban-Rural Development of the People"s Republic of China, Standard for Design of Steel Structures. GB50017-2017. Beijing, 2017.
[23] Ministry of Housing and Urban-Rural Development of the People"s Republic of China, Code for Seismic Design of Buildings. GB50011-2010. Beijing, 2010.
[24] J. Wang, W. Wang, X. Qian, Progressive collapse simulation of the steel-concrete composite floor system considering ductile fracture of steel, Eng. Struct. 200 (2019) 109701.
[25] L. Li, W. Wang, Y. Chen, et al., Experimental investigation of beam-to-tubular column moment connections under column removal scenario, J. Constr. Steel Res. 88 (2013) 244–255.
[26] X. Qin, W. Wang, Y. Chen, et al., Experimental study of through diaphragm connection types under a column removal scenario, J. Constr. Steel Res. 112 (2015) 293–304.
[27] ASCE 7-16, Minimum Design Loads and Associated Criteria for Buildings and Other Structures, Reston, Virginia, American Society of Civil Engineers, 2017.
[28] Y. Bao, J.A. Main, S.Y. Noh, Evaluation of structural robustness against column loss: methodology and application to RC frame buildings, J. Struct. Eng. 143 (8) (2017), 04017066, .